Proc. 13th Int. Symp. on Unmanned Untethered Submersible Technology (UUST), August 2003

Underwater Glider Model Parameter Identification

Joshua G. Graver and Ralf Bachmayer and Naomi Ehrich Leonard*
Mechanical and Aerospace Engineering
Princeton University
Princeton, NJ 08544
jggraver@princeton.edu, ralf@princeton.edu, naomi@princeton.edu

David M. Fratantoni
Physical Oceanography, Mail Stop: 21
Woods Hole Oceanographic Institution
Woods Hole, MA 02543
dfratantoni@whoi.edu

Abstract

An underwater glider is a buoyancy-propelled, fixed-wing vehicle with attitude controlled completely, or in part, by means of internal mass redistribution. We have developed a physics-based nonlinear model of the dynamics of an underwater glider and adapted it to model the SLOCUM glider's geometry, rudder, ballast pump and internal movable mass. In this paper we identify the model parameters to match the steady glides in new flight test data from the SLOCUM glider. In the process we also estimate the buoyancy trim offset of the glider used in the flight tests.

1 Introduction

An underwater glider is a buoyancy-propelled, fixed-wing autonomous underwater vehicle. Attitude is controlled by means of internal mass redistribution and in some cases with external control surfaces. Initially conceived by Henry Stommel [12], autonomous underwater gliders offer many advantages in ocean sensing: long duration missions, greater operational flexibility and low-cost operations. Gliders are more mobile and flexible than fixed moorings, are more maneuverable than drifters, have greater range than other AUV's, and do not need expensive support vessels.

*Research partially supported by the Office of Naval Research under grants N00014–02–1–0826 and N00014–02–1–0861.

Several oceangoing gliders are operational or under development, including the SLOCUM glider [15], the Spray glider [11] and Seaglider [1]. These three gliders are designed for long-duration, ocean sensing missions. They collect oceanographic data such as water temperature, conductivity, depth, and currents. They can also carry other scientific sensors, such as fluorometers, optical backscatter or bioluminescence sensors. The three gliders are similar in size and geometry, each measuring approximately two meters in length and weighing around 50kg. Each has a cylindrical hull, two fixed wings and a tail. All are designed to be statically stable in a glide. The gliders control pitch by moving an internal mass or battery. In the Spray, Seaglider and the thermally powered SLOCUM, roll is also controlled by moving an internal mass or battery. Yaw and heading are controlled through the hydrodynamic yawing moment due to the roll. Some of these gliders are capable of dives to depths of 1,500 meters. In the electric SLOCUM, designed for shallower dives from five to 200 meters and thus more inflections (transition between downwards and upwards glides), roll is set by the glider's static CG position and pitch is controlled by moving internal mass. Yaw and heading are controlled using the rudder mounted on the vertical tail of the glider.

Our research on glider dynamics aims to develop a widely applicable, model-based approach to design and control of gliders. This approach, described in [7] and [3] considers a three-dimensional nonlinear dynamic model of a glider, with hydrodynamic forces, ballast control, internal moving mass control, and nonlinear coupling between the vehicle and movable

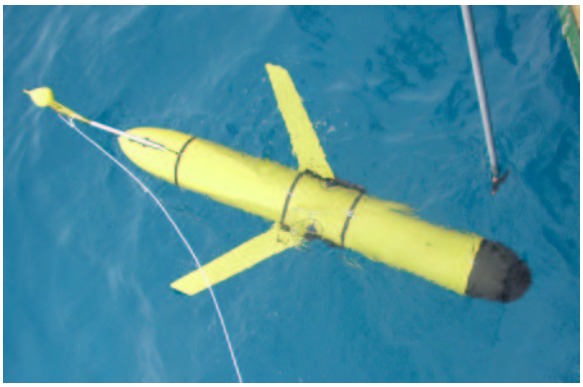

Figure 1: A SLOCUM Glider.

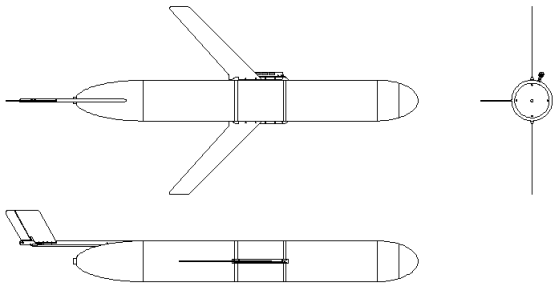

Figure 2: SLOCUM Electric Glider Layout [14].

internal mass. This model is applicable to glider design, to the study of stability and controllability of glide paths and to the derivation of feedback control laws. It is emphasized that this approach is intended to be general rather than vehicle specific and is meant to complement other efforts towards analysis and design of gliders including the SLOCUM, Spray and Seaglider.

In this paper we describe model parameter identification for the SLOCUM using experimental flight test data, focusing in particular on data from steady straight glides. We have adapted our model to the SLOCUM electric glider, modelling the location of the ballast system, the properties of the moving pitch mass, and the rudder. The resulting equilibrium equations appear in Section 2.3. In Section 3 we determine parameter values such that the model will match the data set of equilibria for the glider. This determines the coefficients for our quasi-steady hydrodynamic model and parameters representing the trim and buoyancy of the glider. We discuss next steps and final remarks in Section 4.

2 SLOCUM Glider Model

2.1 SLOCUM Glider

The SLOCUM glider is manufactured by Webb Research Inc., Falmouth, MA, is a buoyancy-driven, autonomous underwater vehicle [13, 15]. The operational envelop of the glider includes a 200 m depth capability and a projected 30 day endurance, which translates into approximately 1000 km operational range with a 0.4 m/s fixed horizontal and 0.2 m/s vertical speed. The glider has an overall length of 1.5 m and a mass of 50 kg. The buoyancy engine is an electrically powered piston drive, located in the nose section of the glider, Figure 1. The drive allows the glider to take in and expel water, thereby changing its overall buoyancy. The mechanism allows a close to neutrally buoyant trimmed glider to change its displacement in water by ± 250 ccm, which corresponds to approximately $\pm 0.5\%$ of the total volume displaced. This change in buoyancy generates a vertical force which is translated through two swept wings into a combined forward and up/downward motion. Due to the location of the piston drive, also called buoyancy engine, the change in direction of the buoyant force also creates the main pitching moment for the glider. Besides the buoyancy engine the glider possesses two more control actuators, a 9.1 kg battery pack, referred to as *sliding mass*, that can be linearly translated along the main axis of the glider and a rudder attached to the vehicle tail fin structure. The sliding mass is used for fine tuning the pitch angle.

The glider has two onboard computers, a control computer and a science computer. Navigation sensors on the glider measure heading, pitch, roll, depth, sliding mass position and the piston drive position. Besides other internal states and other sensor measurements, these readings are recorded and processed by the control computer. Vehicle position at the surface is determined by a GPS receiver, with the antenna located on the rear fin. Note that, while submerged, the glider velocity and horizontal position are not sensed because of the difficulty in measuring these states. While underwater, the glider navigates using a deduced reckoning algorithm. At present, the pitch angle and depth rate measurements and an assumed angle of attack are used by the onboard computer to estimate the horizontal speed of the glider.

The SLOCUM glider can be programmed to navigate in various ways. For a typical mission scenario

the glider navigates to a set of preprogrammed waypoints downloaded prior to execution in a mission specification file and operates under closed-loop pitch and heading control. A mission is composed of yos and segments. A yo is a single down/up cycle, while a segment can be composed of several yos and starts with a dive from the surface and ends with a surfacing. At all surfacings the glider tries to acquire its GPS location. On the surface the glider compares its desired waypoint to its actual GPS position and determines a heading correction for the next waypoint before it dives again for the next segment of the mission. Other modes of operation such as gliding at a given compass heading, fixed rudder angle or fixed battery position are easy to implement and were used in the work presented in this paper.

2.2 Experiments with SLOCUM

We conducted glider in-water flight tests during January 2003 near Chub Key, Bahamas, using SLOCUM Glider WE01, owned and operated by Woods Hole Oceanographic Institution (WHOI). The principal investigator on this research cruise was Dr. David Fratantoni from Woods Hole Oceanographic Institution, Woods Hole, MA. Operations were conducted from the RV Walton Smith of the University of Miami. Using glider WE01, we conducted a series of test glides including both steady straight and turning glides and glides with more dynamic behavior.

The glider experiments conducted on the cruise were designed for model confirmation and parameter identification. The hydrodynamic properties of the SLOCUM glider were estimated in advance using theoretical calculations and standard aerodynamic reference data. In order to collect the necessary data, we performed a set of glides including (1) steady glides at different pitch angles and (2) glides that exhibit rich dynamic behavior such as unsteady turning and pitching with large actuator excursions.

A typical flight test mission consisted of two glides to fifty meters depth, enough depth to reach equilibrium glides. The glider surfaced at the beginning and end of the mission for a GPS position fix and data transfer. Both fixed control glides and glides using pitch and heading feedback were conducted. During fixed control glides, the rudder and sliding pitch mass are held at pre-determined positions for the duration of each downwards and upwards glide. This resulted in the glider reaching a steady glide equilibrium corresponding to those control settings.

Although there is always some state disturbance and measurement noise in the data, the steady glides stand out plainly (see Figures 3 and 4). Choosing the

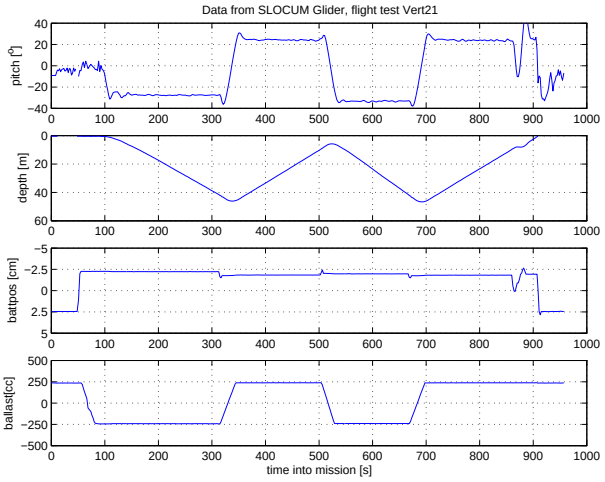

Figure 3: SLOCUM Data from Flight Test.

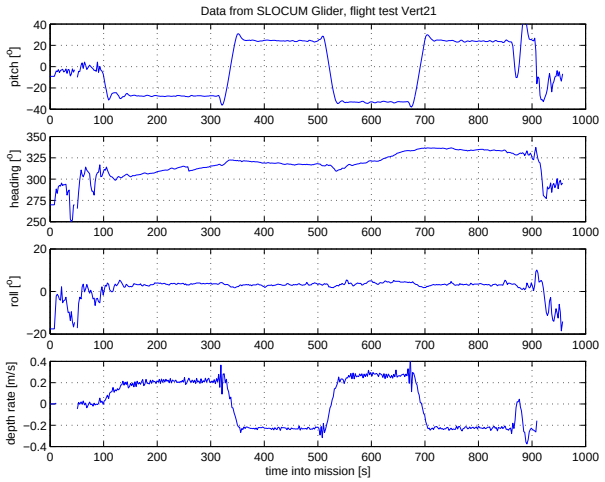

Figure 4: SLOCUM Data from Flight Test.

steady glides in the data and computing the average state over the interval of the steady glide gives a set of steady glides. As an example, average state values for four steady glides are shown in Table 1, as are values for α, V and $C_D(\alpha_{eq})$ by frontal area computed using methods described in Section 3.

There are a number of sources of uncertainty in the flight test data. As noted, the glider velocity and horizontal position are not measured. The current conditions in the area of operation are unknown. Estimates of the current may be made using the model of the glider dynamics, but this cannot be used to determine the model parameters. Glider velocity and current are important because the hydrodynamic forces on the glider depend on the glider speed relative to the water. Other sources of uncertainty in the glider data include the trim condition of the glider and the CG

Avg. Value	Glide 1	Glide 2	Glide 3
Pitch θ (deg)	-22.77	23.74	-25.78
Depth rate $\dot{z}$ (m/s)	0.168	-0.224	0.200
Battery pos. (cm)	-2.4	-1.8	-2.3
Ballast m_b (cc)	244.4	-237.3	247.7
Rudder δR (deg)	2	4	2
Roll ϕ (deg)	3.34	3.23	3.81
Heading ϕ (deg)	334	333	333
AoA α (deg)	2.7	-2.9	2.3
Speed V (m/s)	0.388	0.499	0.425
Drag Coeff. $C_D(\alpha_{eq})$	0.27	0.31	0.25

Table 1: Example of Steady Glide Data.
Flight Vert22_4 on SLOCUM Glider WE01.

position. Some static roll offset appears in the data, i.e. the CG and static trim of the glider induced some static roll. Because of operational considerations during the cruise it was not possible to correct this trim or to obtain completely accurate static mass and trim measurements. The wings are made of a thin composite material which may deflect during flight and change the predicted flight performance. When at the surface to determine GPS position, the glider is subject to wind and current-driven drifting, and this leads to some uncertainty in the glider's surfacing position.

Our analysis is designed to minimize the effects of these uncertainties, making as much use as possible of the directly measured states. For example, GPS positions are not used in the calculation of the glider velocity.

As mentioned above, the glider used in experiments had a slight static roll due to miss-trim. Because of this, the glider is slightly out of the longitudinal plane in flight. This is another possible source of error in the experimental analysis. The static roll produces a small yaw moment which is offset by a small rudder angle. This probably results in the glider flying with some sideslip angle. This could result in additional drag on the glider and possibly change the lift and moment on the glider in comparison with fully longitudinal, zero-sideslip flight. These problems could be reduced in future flight tests by correcting the roll trim of the glider.

2.3 SLOCUM Model Planar Equilibrium Equations

We have derived a model of glider dynamics, described in [7] and [3]. Our dynamic glider model describes a glider with simple body and wing shape. Control is applied to two point masses inside the vehicle: we control the mass of a point with fixed position in the body, representing the ballast tank, and control the position of a mass with varying position within the body, representing the moving battery pack. The model describes the nonlinear coupling between the vehicle and the shifting and changing masses. The major forces on a glider are all incorporated into the model, including buoyancy, the moments and forces due to the internal moving mass, and quasi-steady hydrodynamic forces. Beginning with the glider equations from [7], we add terms to the model to account for the SLOCUM ballast system location, the sliding mass range of travel, and the rudder. The aim of the model is to adequately match the dynamic performance of the glider while maintaining a level of simplicity in the model that allows for analytical work and design insight.

We take the glider hull to be symmetrical with wings and tail attached so that the center of buoyancy (CB) is at the center of the hull. We assign a coordinate frame fixed on the vehicle body to have its origin at the CB and its axes aligned with the principle axes of the hull. Let body axis 1 lie along the long axis of the vehicle (positive in the direction of the nose of the glider), let body axis 2 lie in the plane of the wings and body axis 3 point in the direction orthogonal to the wings as shown in Figure 5.

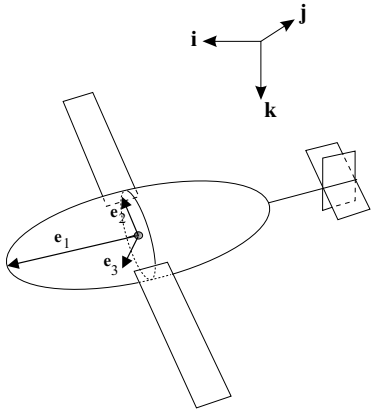

Figure 5: Frame assignment on underwater glider.

The total stationary mass of the glider, m_s, (also referred to as body mass) is the sum of three terms: $m_s = m_h + m_w + m_b$. m_h is a fixed mass that is uniformly distributed throughout the body of the glider, m_w is a fixed point mass that may be offset from the CB, and m_b is the variable ballast point mass, also offset from the CB in the SLOCUM. $m_s = m_h + m_w + m_b$. The vector from the CB to the point mass m_w is $\boldsymbol{r_w}$. The vector from the CB to the variable ballast mass m_b is $\boldsymbol{r_b}$. The moving

internal point mass is $\bar{m}$. The vector $\boldsymbol{r_p}(t)$ describes the position of this mass with respect to the CB at time t. The total mass of the vehicle is then

$$m_v = m_h + m_w + m_b + \bar{m} = m_s + \bar{m}.$$

The mass of the displaced fluid is denoted m and we define the net buoyancy to be $m_0 = m_v - m$ so that the vehicle is negatively (positively) buoyant if m_0 is positive (negative). The different masses and position vectors are illustrated in Figure 6.

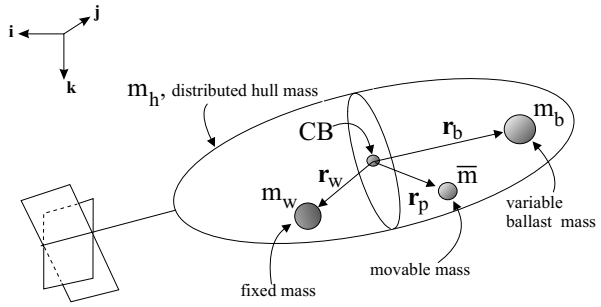

Figure 6: Glider mass definitions.

Here we consider this model specialized to the longitudinal plane (assumed invariant), as in [7], and solve for the equilibrium steady glides in the equations of motion. The resulting SLOCUM vertical plane equilibrium equations are

$$\begin{aligned}
\dot{x} &= v_1 \cos\theta + v_3 \sin\theta && (1)\\
\dot{z} &= -v_1 \sin\theta + v_3 \cos\theta && (2)\\
0 &= (m_{f3} - m_{f1}) v_{1_{eq}} v_{3_{eq}} \\
&\quad -\bar{m} g (r_{P1_{eq}} \cos\theta_{eq} + r_{P3_{eq}} \sin\theta_{eq}) \\
&\quad -m_{b_{eq}} g (r_{B1} \cos\theta_{eq} + r_{B3} \sin\theta_{eq}) \\
&\quad -m_w g (r_{W1} \cos\theta_{eq} + r_{W3} \sin\theta_{eq}) \\
&\quad +M_{DL_{eq}} && (3)\\
0 &= L_{eq} \sin\alpha_{eq} - D_{eq} \cos\alpha_{eq} - m_{0_{eq}} g \sin\theta_{eq} && (4)\\
0 &= L_{eq} \cos\alpha_{eq} + D_{eq} \sin\alpha_{eq} - m_{0_{eq}} g \cos\theta_{eq} && (5)
\end{aligned}$$

where the subscript eq denotes the state at equilibrium steady glide. v_1 and v_3 are the components of the glider velocity in the $\boldsymbol{e_1}$ and $\boldsymbol{e_3}$ directions, respectively, as shown in Figure 5. Here, θ is pitch angle, α is the angle of attack, D is drag, L is lift and M_{DL} is the viscous moment as shown in Figure 7. m_{f3} and m_{f1} are the added mass terms corresponding to the $\boldsymbol{e_1}$ and $\boldsymbol{e_3}$ directions, as derived by Kirchhoff [6]. In these equations, as in [7], we take the added mass cross terms to be zero. We note that equilibrium terms corresponding to the offset mass m_w and the location $\boldsymbol{r_B}$ of the ballast mass m_b do not appear in our earlier model, [7].

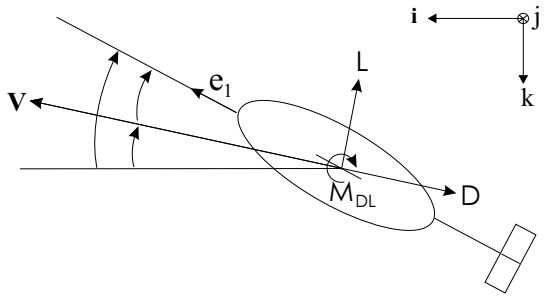

Figure 7: Lift and drag on glider.

As shown in Figure 7, we denote the glide path angle by ξ where

$$\xi = \theta - \alpha.$$

At equilibrium, it may be shown that

$$\xi_{eq} = -\tan^{-1}\left(\frac{D_{eq}}{L_{eq}}\right)$$

We also denote the glider speed by V where

$$V = \sqrt{(v_1^2 + v_3^2)}.$$

Using Equation (2) and our angle definition in Figure 7, we can write the glider depth rate as

$$\dot{z} = -V \sin(\xi) = -V \sin(\theta - \alpha) \qquad (6)$$

The hydrodynamic forces and moment are modelled as

$$D = \frac{1}{2}\rho C_D(\alpha) A V^2 \approx (K_{D_0} + K_D \alpha^2)(v_1^2 + v_3^2) \quad (7)$$

$$L = \frac{1}{2}\rho C_L(\alpha) A V^2 \approx (K_{L_0} + K_L \alpha)(v_1^2 + v_3^2) \quad (8)$$

$$M_{DL} = \frac{1}{2}\rho C_M(\alpha) A V^2 \approx (K_{M_0} + K_M \alpha)(v_1^2 + v_3^2) \quad (9)$$

where C_D, C_L and C_M are the standard aerodynamic drag, lift and moment coefficients by cross sectional area, A is the maximum glider cross sectional area, and ρ is the fluid density. For the longitudinal quasi-steady fluid model, C_D, C_L and C_M are functions of α and the K's are constant coefficients. This model is a standard one, derived using airfoil theory and potential flow calculations and then verified using experimental observations, see for example [2, 8]. A method for determination of the coefficients is described in Section 3.

This quasi-steady hydrodynamic model is expected to be accurate for equilibrium steady glides. It may

be less accurate away from equilibrium glides and when the glider experiences high accelerations or angular rates. The hydrodynamics of the flow about the glider are much more complex during such motions, requiring a more complex hydrodynamic model. In the case of our initial analysis and the standard mission use of the SLOCUM glider, the majority of the operational time is spent at steady glides. Transitions and inflections between steady glide equilibria are relatively slow and gradual. Because of this, the quasi-steady hydrodynamic model may prove satisfactory for our analysis. Incorporating a more complex hydrodynamic model involves adding terms to the lift, drag and moment model.

An analysis of the equilibrium steady glide equations for a generic glider appears in [7]. One interesting property of the equilibrium steady glide equations is that the glide path angle is independent of the glide speed. Glide path angle depends only on the equilibrium angle of attack. When choosing an equilibrium glide, it is possible to specify the glide path angle, determine the required angle of attack, and then choose a glide speed V. The glide speed depends on the net buoyancy of the glider, set by the ballast control and the glide hydrodynamics.

Determining the steady glides for a glider such as the SLOCUM requires finding the set of model parameters that describe the glider mass and hydrodynamic characteristics. This is described in Section 3 Using one method, the hydrodynamic coefficients of the glider are estimated using reference data for ships, submarines and standard shapes. With these estimated coefficients, the equilibrium equations may be used to compute the set of steady glide conditions for the SLOCUM glider. Figure 8 shows the steady glide angles given the estimated lift and drag parameters. Figure 9 shows the steady glide speeds given the same estimated parameters.

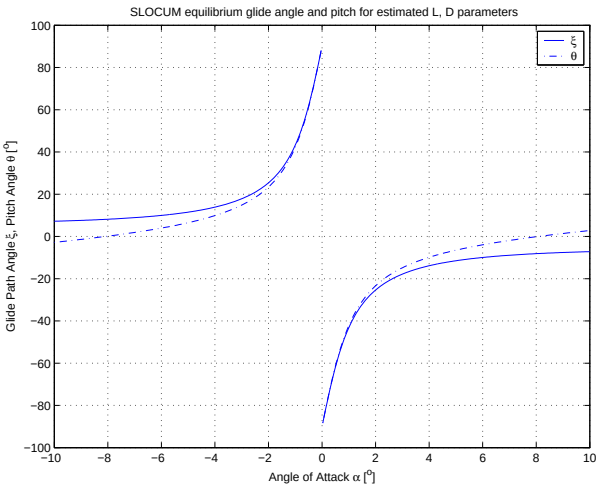

Figure 8: Equilibrium glides using lift, drag, estimated from reference data.

3 Parameter Identification

We wish determine the model parameters matching the SLOCUM model equilibria equations (1)-(5) to the steady glides from data. These parameters represent the physical variables corresponding to the glider's mass, inertia and hydrodynamic characteristics. The parameters that appear in the steady glide equations are the displacement m, the masses m_h, m_w, and $\bar{m}$, the positions $\boldsymbol{r_B}$ and $\boldsymbol{r_W}$ of the ballast mass and offset mass, and the hydrodynamic parameters K_{D_0}, K_D, K_{L_0}, K_L, K_{M_0}, K_M, m_{f3} and m_{f1}.

Parameters corresponding to mass and inertia may be measured directly. The mass and buoyancy trim of the glider can be measured by weighing the glider in air and in water. The position of the glider CG may be determined through direct experimental measurement. The position of the CB is the centroid of the displaced volume of water, and can be computed from the glider geometry. Other mass parameters can be determined using similar methods. The inertia characteristics of the glider can be measured several ways; one way is the bifilar pendulum method, which uses the glider's frequency of oscillation in a pendulum apparatus. Note that the moment of inertia does not appear in the equilibrium equations.

If direct measurement is not possible, for example when a glider is already at sea, it may be possible to determine some of these parameters through analysis of glider data and by comparison of several equilibria. For example, in Section 3.2 we describe a method to identify a glider's buoyancy trim offset from flight test data and in Section 3.3 we use an analogous method to identify the glider static pitch trim.

A variety of methods were used to determine model hydrodynamic parameters, including reference hydrodynamic data for generic shapes, aircraft, ships and submarines, computational fluid dynamics (CFD) analysis, wind tunnel data, and flight test data. An extensive selection of references is available, including [4], [6] and [10]. Because the hydrodynamic parameters are sensitive to small changes in the vehicle geometry, the challenge in determining these parameters is to accurately match actual flight data.

We first estimated hydrodynamic parameters for lift, drag and moment for the SLOCUM geometry using reference data. This involved calculating the hydrodynamic forces on each of the glider compo-

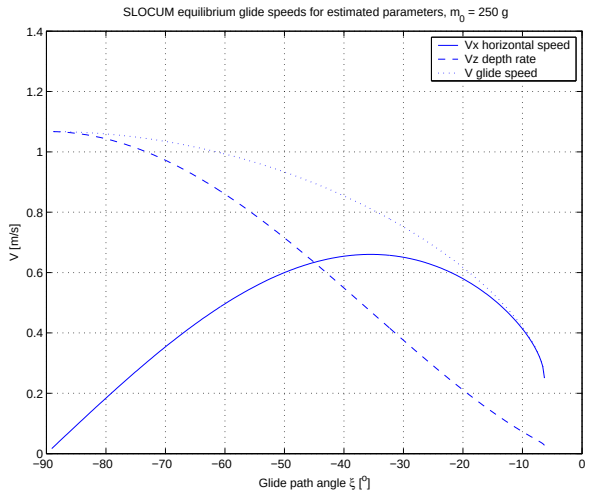

Figure 9: Equilibrium speed using lift, drag, estimated from reference data.

nents using theoretically and experimentally determined reference data. These parameters were compared to the results of our preliminary wind tunnel tests conducted at Princeton. More accurate wind tunnel tests are in progress using the methods of [9]. In addition, calculations of glider hydrodynamic characteristics using CFD analysis appear in [5].

Solving Equation (6) for V gives

$$V = \left| \frac{\dot{z}}{\sin(\theta - \alpha)} \right| \tag{10}$$

Substituting Equation (10) and the hydrodynamic coefficients (7), (8), and (9) into Equations (4) and (5) gives us

$$\begin{aligned} 0 &= \frac{1}{2}\rho C_L(\alpha_{eq}) A \left(\frac{\dot{z}_{eq}}{\sin(\theta_{eq} - \alpha_{eq})} \right)^2 \sin \alpha_{eq} \\ &\quad - \frac{1}{2}\rho C_D(\alpha_{eq}) A \left(\frac{\dot{z}_{eq}}{\sin(\theta_{eq} - \alpha_{eq})} \right)^2 \cos \alpha_{eq} \\ &\quad - m_{0_{eq}} g \sin \theta_{eq} \end{aligned} \tag{11}$$

$$\begin{aligned} 0 &= \frac{1}{2}\rho C_L(\alpha_{eq}) A \left(\frac{\dot{z}_{eq}}{\sin(\theta_{eq} - \alpha_{eq})} \right)^2 \cos \alpha_{eq} \\ &\quad + \frac{1}{2}\rho C_D(\alpha_{eq}) A \left(\frac{\dot{z}_{eq}}{\sin(\theta_{eq} - \alpha_{eq})} \right)^2 \sin \alpha_{eq} \\ &\quad - m_{0_{eq}} g \cos \theta_{eq} \end{aligned} \tag{12}$$

These equations include measured quantities $\dot{z}$, θ and m_0. Angle of attack α is a function of v_1 and v_3 and is not sensed. Hydrodynamic coefficients $C_L(\alpha)$ and $C_D(\alpha)$ have been estimated but are not known exactly. These estimates, however, do yield forces in the form (7) and (8). Substituting (7) and (8) into (11) and (12) gives two equations with four parameters K_{D_0}, K_D, K_{L_0}, K_L and unknown α. We use an existing estimate the value of the lift parameters and then determine drag parameter values consistent with the flight test data. This is necessary because of the limited number of states available from the glider. Angle of attack or velocity data would allow us to determine more parameters from experimental data.

3.1 Lift

The SLOCUM glider body is symmetric from top to bottom and the wings are symmetrical flat plates. From this, the reference methods show that lift should be zero at angle of attack $\alpha = 0$ and should be antisymmetric about $\alpha = 0$. We compared estimates of the lift coefficient of the glider from three sources: aerodynamic reference data, CFD analysis from [5], and preliminary wind tunnel data. These estimates are reasonably close to one another. The lift coefficient from [5] was computed using the most advanced methods, so we use this estimate for $C_L(\alpha)$ by frontal area:

$$C_L(\alpha) = 11.76\,\alpha + 4.6\,\alpha|\alpha| \tag{13}$$

where α is in radians. Note that this is close to, but not exactly, linear in α as modelled in (8).

Equations (11) and (12) may be rearranged, given glider lift coefficient (13) and the steady-glide-test sensor data described in Section 2.2. Solving (12) for drag D_{eq} and substituting into (11) gives

$$\begin{aligned} 0 &= L_{eq} \sin \alpha_{eq} - m_{0_{eq}} g \sin \theta_{eq} \\ &\quad - \left(\frac{L_{eq} \cos \alpha_{eq} - m_{0_{eq}} g \cos \theta_{eq}}{\sin \alpha_{eq}} \right) (\cos \alpha_{eq}), \\ \text{where} \quad L_{eq} &= \frac{1}{2}\rho C_L(\alpha_{eq}) A \left(\frac{\dot{z}_{eq}}{\sin(\theta_{eq} - \alpha_{eq})} \right)^2. \end{aligned}$$

This equation may be solved for the angle of attack from flight data for a given steady glide.

3.2 Drag

In this section we determine a drag coefficient for the glider given (13), such that steady glides computed with the equilibrium equations are consistent with flight test data. We describe first an analysis using the buoyancy tank ballast m_b as the glider net buoyancy m_0. This yields a $C_D(\alpha)$ that is inconsistent with our expected drag in both form and magnitude, as discussed below. We then describe a method used

to identify a static buoyancy trim offset in the test glider. The buoyancy trim offset is then used to compute a $C_D(\alpha)$ that is more consistent with theoretical and other predictions.

Drag estimates calculated using aerodynamic reference methods or preliminary wind tunnel tests each predict that glider drag coefficient $C_D(\alpha)$ will have the form given in Equation (7). Because of the glider's symmetrical design, drag should be symmetrical (an even function) with respect to angle of attack, with the minimum (profile) drag at zero angle of attack.

Using Equation (11) or (12), one can solve for $C_D(\alpha_{eq})$ given data for a steady glide and the lift and angle of attack from Section 3.1. Figure 10 shows the drag coefficient determined for each glide in the set of steady glides from test data. Each point on the plot corresponds to the coefficient of drag calculated for one steady glide.

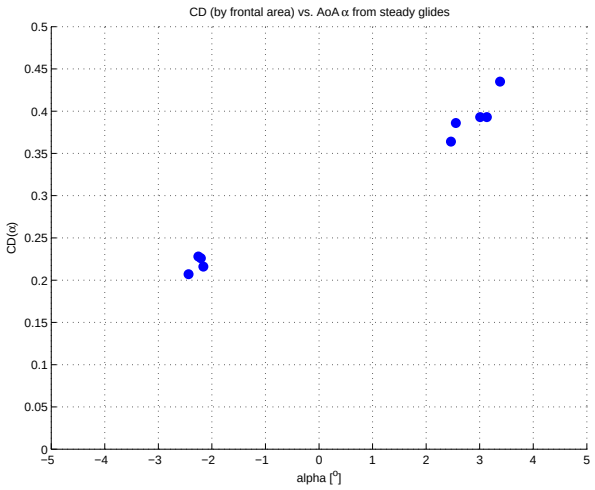

Figure 10: C_D computed from equilibrium glide data assuming no buoyancy trim offset.

Note that glides with positive angle of attack α, which are glides downwards, have much higher coefficients of drag than the group of glides upwards glides with negative angles of attack. This result is not consistent with any of the estimates for the glider drag dependence on α. Our reference calculation of drag predicts a parabolic drag dependence on angle of attack. The drag shown is also higher than the predicted drag.

One possible explanation for the differences between upwards and downwards glide is that the glider actually has an asymmetrical drag curve. Some elements of the glider geometry are asymmetrical from top to bottom, including the CTD sensor located below one of the wings and the vertical tail. However, these items are small compared to the glider body and wings, both of which are symmetrical, so it is not expected that these small differences would account for such a large difference in the drag. Regardless of this asymmetry, drag is still expected to be close to minimum at zero angle of attack.

The simplest and the most obvious explanation for the difference between the upwards and downwards glides is an offset in the glider buoyancy trim. This offset can be found using the symmetry of the glider and lift coefficient to compare upwards and downwards glides at the same magnitude pitch angles. As noted, because of the symmetrical design of the glider, the lift curve is an odd function with respect to angle of attack and the drag curve is expected to be an even function, see Figure 8.

Glides conducted at the same magnitude pitch angle upwards and downwards should have the same magnitude glide path angle ξ_{eq} and angle of attack α_{eq}. Given the symmetry in lift and drag, and our approximation to the longitudinal plane, differences in velocity between these glides are caused by differences in the driving buoyant force. By comparing such glides in the flight test data, we estimate the trim offset in the glider buoyancy.

First we substitute $m_{0_{eq}} = m_{b_{eq}} + \triangle m_0$ into Equation (14). Using the steady glide data, we estimate the buoyancy trim offset $\triangle m_0$ by requiring glides with the same $|\theta_{eq}|$ to have the same $|\alpha_{eq}|$. This involves solving for α_{eq} for each of the symmetrical glides as a function of $\triangle m_0$ and determining the $\triangle m_0$ for equal $|\alpha_{eq}|$. Using the available data, we estimate the buoyancy trim offset to be $\triangle m_0 = -73$ grams. This means that, for the water density and the weight of the glider WE01 during these tests, the glider is 73 grams light (positively buoyant) when the ballast tank is set at the half full, $m_b = 0$, "zero buoyancy" point. When this buoyancy trim offset is not accounted for, as shown in Figure 10, it appears that there is more drag going down (i.e., it is harder to go down) and less drag going up (i.e., easier).

Substituting $m_{0_{eq}} = m_{b_{eq}} + \triangle m_0$ into Equations (11) or (12), $C_D(\alpha_{eq})$ may be computed for each steady test glide, see Figure 11.

A least-square fit of the data, assuming drag of the form (7), gives drag parameter

$$C_D(\alpha) \quad = \quad 0.214\,\alpha + 32.3\,\alpha^2. \qquad (14)$$

where α is in radians. As shown in Figure 11, the steady-glide data points are close to a parabolic function of angle of attack α and are symmetrical about $\alpha = 0$. These properties are consistent with the expectations from our reference calculations for drag.

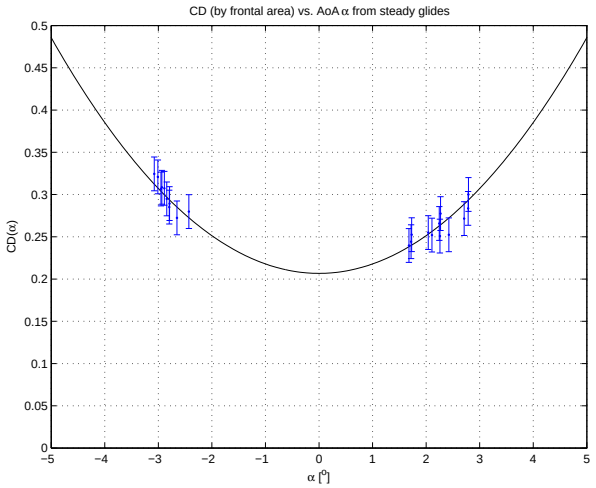

Figure 11: C_D computed from equilibrium glide data assuming buoyancy trim offset of - 73 grams.

The magnitude of the drag least-squares fit (14) is about 75% greater, at $\alpha = 0$, than the drag calculated from references, and as much as 150% greater at $\alpha = -3^o$. There are several possible explanations for the difference between the drag found here and the drag predictions using reference calculations. One explanation is that the drag model is based on an ideal geometric model and does not include variations in the geometry (e.g. surface roughness, wing deformation, ...), protrusions and additions such as the CTD sensor. The model therefore does provide a drag estimate that is lower than the measured drag. Another possible explanation is that the steady glides measured in the flight data deviate from the longitudinal plane. This is highly probably because of the glider static roll miss-trim. It can be seen in the flight test data that, when the glider is set to glide with rudder fixed at zero, there is some small yaw rate. This shows that at least some of the glides have a nonzero sideslip angle. Because the glider has no sideslip and angle of attack sensors, the order of the sideslip angle must be estimated from other sensor data. By examining the data it may be seen that the yaw rates are very low in these cases, suggesting the sideslip angle is small and that its effects on the glider yaw rate are small. In other test glides a small rudder angle was used and was enough to offset the yaw rate due to roll. It is possible that this sideslip angle due to the static roll is of the same order of magnitude as the angle of attack, and may account for the differences between the expected and estimated drag. The difference may also be explained by a combination of these factors. This is a continuing subject of analysis.

Using the hydrodynamic coefficients determined from the data, the equilibrium equations may be used to compute a new set of steady glide conditions, as was done for Figures 8 and 9 using the estimated parameters. Figure 12 shows the steady glide angles given the parameters identified from the data. Figure 13 shows the steady glide speeds given the same identified parameters. For a 25^o glide angle, the identified parameters yield a depth rate of 20 cm/s and a horizontal speed of 42 cm/s, as can be seen from Figure 13. This is consistent with estimates from glider operations conducted by Webb Research Corporation and WHOI.

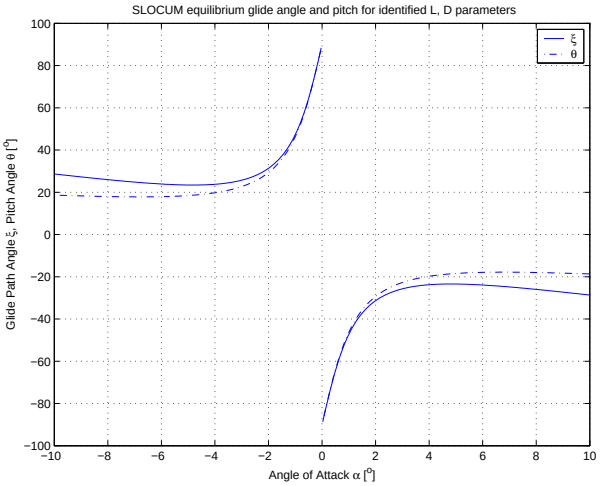

Figure 12: Equilibrium glides using Lift, Drag fit to data

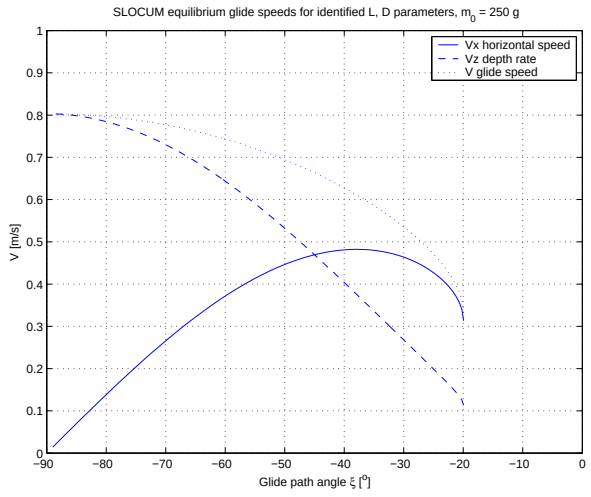

Figure 13: Equilibrium speed using Lift, Drag fit to data.

3.3 Pitch Moment

To compute the hydrodynamic moment on the glider during steady flight, we use Equation (3). The moments due to the internal mass, the ballast tank and the offset mass may be computed from the steady-glide sensor data. Other terms in Equation (3) represent the hydrodynamic moments due to the glider's added mass and the rest of the glider hydrodynamics. For the steady-state analysis, we will group these terms together as

$$\frac{1}{2}\rho AV^2 C_M(\alpha) = (m_{f3} - m_{f1}) v_{1_{eq}} v_{3_{eq}} + M_{DL_{eq}}. \quad (15)$$

Substituting (15) into Equation (3) and rearranging gives

$$\begin{aligned}\frac{1}{2}\rho AV^2 C_M(\alpha) &= (\bar{m}g(r_{P1_{eq}} \cos\theta_{eq} + r_{P3_{eq}} \sin\theta_{eq}) \\ &+ m_{b_{eq}} g(r_{B1} \cos\theta_{eq} + r_{B3} \sin\theta_{eq}) \\ &+ m_w g(r_{W1} \cos\theta_{eq} + r_{W3} \sin\theta_{eq})) \quad (16)\end{aligned}$$

which may be solved for $C_M(\alpha)$ given the steady glide flight data.

During trimming of the glider before a mission, static weights are positioned within the hull and instruments may be installed or moved. This changes the mass and trim of the glider. In the model, the uniformly distributed hull mass m_h and the offset mass m_w represent the distribution of fixed components in the glider. The position of the offset mass may be determined using static measurements during trimming of the glider before launch, or calculated from flight test data. Before launch the SLOCUM gliders are trimmed manually using a static buoyancy tank. The glider ballast tank is set to half-full and weights are adjusted within the hull to make the glider neutrally buoyant and level. Using data from the static trim process, we may determine m_w and $\boldsymbol{r_w}$ by solving Equation (3) with $v_1 = 0$ and $v_3 = 0$. The mass and position of the ballast and sliding mass are determined from flight test sensor data.

In some cases, as discussed in Section 3.2, it may not be possible to measure the static trim of the glider. In this case it is possible to determine the mass offset r_{W1}, given r_{W3} and a set of data from symmetrical steady glides up and down. Using a method of comparison analogous to that in Section 3.2, we use the symmetry of the glider to compare upwards and downwards glides at the same pitch angle. To estimate r_{W1} we use the sensor state data from these glides and first compute the moment due to internal masses (as a function of unknown r_{W1}) for each glide. This is set equal to the hydrodynamic moment according to (3) for each glider. We then equate the magnitude of the moment coefficients for an upward glide and a downward glide corresponding to the same pitch angle magnitude and solve for r_{W1}. For glider WE01 as trimmed in these tests, this analysis gives $r_{W1} = -0.093\ m$.

Once we have determined the internal masses and positions, we may solve for $C_M(\alpha)$ for each glide in our set of steady glides. The result and a least squares fit are shown in Figure 14.

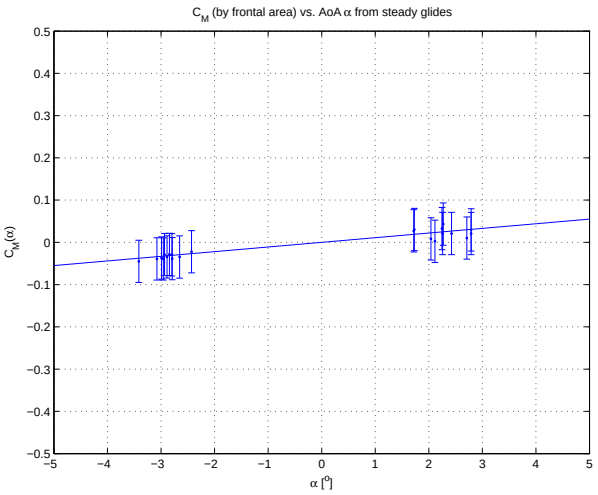

Figure 14: C_M computed from equilibrium glide data.

The least-square fit of this data, using the form given in Equation 9 with $K_{M_0} = 0$ because of the symmetry of the glider, is

$$C_M(\alpha) = 0.63\,\alpha.$$

where α is in radians.

The hydrodynamic moment on the glider is small compared to the moments due to the internal masses. The moment due to the ballast and sliding mass together is around 35 N·m in the nose-down direction. The offset mass, located behind the vehicle CB, provides a countering nose-up moment. At equilibrium, the hydrodynamic moment is the difference between these moments, as shown in Equation (16). We estimate the hydrodynamic moment to be of the order 0.1 N·m or less. Because this moment is small in magnitude as compared to the other moments, small uncertainties in the positions of the internal masses result in relatively large uncertainties in the moment coefficient. Note that some variation in $C_M(\alpha)$ would yield plots lying within the error bounds shown in Figure 14. Effects due to glider motion out of the longitudinal plane in some flight tests will also influence the accuracy of the analysis, as noted in Section 3.2. In

order to determine the glider coefficient of moment more accurately, other methods such as wind tunnel tests and CFD analysis may be employed. The relatively small hydrodynamic moment means that, for gliders like SLOCUM travelling at low velocities, the pitching effect of the internal mass controls can easily overcome the vehicle hydrodynamic moment.

4 Final remarks

Once the equilibrium steady glides are matched, the remaining unknown parameters are those that appear only in the dynamic equations of the vehicle and not at the equilibria. To solve for these parameters we make use of a simple metric. The metric defines how the parameters should provide an adequate match of our dynamic model output to the flight test data. The parameters are determined through an iterative process that involves simulating the glider dynamics, measuring the quality of fit to the experimental data using the metric, and adjusting the parameters for a better fit. The process is carried out numerically, using a steepest-descent search method to adjust the model parameters before each iteration and comparison of model output with the flight test data. The results of this analysis will be reported in a future work.

The method, in Section 3.2, for determining the static buoyancy trim offset of the glider could possibly be adapted to trim the glider at the beginning of a deployment and to detect system changes in the glider during deployment. Possible system faults in the glider that could occur during a mission include (1) fouling by seaweed, (2) taking on water through a small leak in the hull or (3) a problem with the ballast system. These faults could be detected and distinguished using the methods described here by comparing upwards and downwards glides.

The results and analysis of the flight data used in this paper suggest benefits to making use of additional sensors and methods for future flight tests. Moorings or fixed sensors located off the glider but in the flight test area could be used to measure the current conditions at the operational depths. For the purpose of flight tests, sensors could be temporarily installed on the glider to measure its velocity and angle of attack. Such sensors are standard in aircraft flight test but would require adaptation for use on the glider, both because it is underwater and travels at a low velocity. During flight testing, position and velocity could both be measured by an acoustic ranging system. Measuring data with high enough accuracy would probably require a purpose-built acoustic range, the use of an existing naval test range or the like. Some acoustic systems are already in the process of being adapted for use on the SLOCUM glider, and these could provide a useful estimate of the glider position and velocity during tests. These sensor systems vary in size and expense, with the use of an existing doppler current measuring installation being relatively inexpensive. It would not be necessary to add these flight test sensors permanently to the glider, but rather install them temporarily for the duration of flight tests. These types of data would allow more accurate measurement of the glider dynamics and hydrodynamic characteristics.

5 Acknowledgements

The first three authors would like to thank David M. Fratantoni from WHOI for the opportunity to join the glider test cruise on board the *RV Walton Smith* in January 2003 and for providing the gliders and assistance in performing the glider flight tests. Thanks also to the captain and crew of the *RV Walton Smith* for their help and support. We would also like to thank Clayton Jones and Douglas C. Webb from Webb Research Corporation and Tom Campbell from Dinkum Software for their expertise and help in all areas related to the SLOCUM gliders.

References

[1] C. C. Eriksen, T. J. Osse, T. Light, R. D. Wen, T. W. Lehmann, P. L. Sabin, J. W. Ballard, and A. M. Chiodi. Seaglider: A long range autonomous underwater vehicle for oceanographic research. *IEEE Journal of Oceanic Engineering, Special Issue on Autonomous Ocean Sampling Networks*, 26(4):424–436, 2001.

[2] B. Etkin. *Dynamics of Flight.* John Wiley and Sons, New York and London, 1959.

[3] J.G. Graver and N.E. Leonard. Underwater glider dynamics and control. In *Proc. 12th Int. Symposium on Unmanned Untethered Submersible Tech.*, Durham, NH, 2001.

[4] S. F. Hoerner. *Fluid Dynamic Drag.* Published by the author, Midland Park, NJ, 1965.

[5] S. A. Jenkins, D. E. Humphreys, J. Sherman, J. Osse, C. Jones, N. E. Leonard, R. Bachmayer, J. Graver, E. Clem, P. Carroll, P. Davis, J. Berry, P. Worley, and J. Wasyl. Underwater glider system study. Technical report, Office of Naval Research, 2003.

[6] H. Lamb. *Hydrodynamics*. Dover, New York, 6th edition, 1932.

[7] N.E. Leonard and J.G. Graver. Model-based feedback control of autonomous underwater gliders. *IEEE Journal of Oceanic Engineering, Special Issue on Autonomous Ocean Sampling Networks*, 26(4):633–645, 2001.

[8] B. W. McCormick. *Aerodynamics, Aeronautics and Flight Mechanics*. John Wiley, New York and London, 1979.

[9] W. H. Jr. Rae and A. Pope. *Low-Speed Wind Tunnel Testing*. John Wiley and Sons, New York, 1984.

[10] J. Roskam. *Methods for Estimating Stability and Control Derivatives of Conventional Subsonic Airplanes*. Published by the author, Lawrence, KS, 1971.

[11] J. Sherman, R. E. Davis, W. B. Owens, and J. Valdes. The autonomous underwater glider 'Spray'. *IEEE Journal of Oceanic Engineering, Special Issue on Autonomous Ocean Sampling Networks*, 26(4):437–446, 2001.

[12] H. Stommel. The Slocum mission. *Oceanography*, 2:22–25, 1989.

[13] D. Webb and C. Jones. Personal communication, 2001.

[14] D. Webb and C. Jones. Slocum electric glider layout. Technical Drawings, 2002.

[15] D. C. Webb, P. J. Simonetti, and C.P. Jones. SLOCUM, an underwater glider propelled by environmental energy. *IEEE Journal of Oceanic Engineering, Special Issue on Autonomous Ocean Sampling Networks*, 26(4):447–452, 2001.